

Convergence acceleration of Navier-Stokes equation using adaptive wavelet method[†]

Hyungmin Kang¹, Imran Ghafoor² and Dohyung Lee^{2,*}

¹School of Mechanical and Aerospace Engineering, Seoul National University, Seoul, 151-742, Korea

²Department of Mechanical Engineering, Hanyang University, Ansan, Kyung-Ki-Do, 425-791, Korea

(Manuscript Received August 3, 2009; Revised October 23, 2009; Accepted November 18, 2009)

Abstract

An efficient adaptive wavelet method is proposed for the enhancement of computational efficiency of the Navier-Stokes equations. The method is based on sparse point representation (SPR), which uses the wavelet decomposition and thresholding to obtain a sparsely distributed dataset. The threshold mechanism is modified in order to maintain the spatial accuracy of a conventional Navier-Stokes solver by adapting the threshold value to the order of spatial truncation error. The computational grid can be dynamically adapted to a transient solution to reflect local changes in the solution. The flux evaluation is then carried out only at the points of the adapted dataset, which reduces the computational effort and memory requirements. A stabilization technique is also implemented to avoid the additional numerical errors introduced by the threshold procedure. The numerical results of the adaptive wavelet method are compared with a conventional solver to validate the enhancement in computational efficiency of Navier-Stokes equations without the degeneration of the numerical accuracy of a conventional solver.

Keywords: Navier-Stokes equations; Adaptive wavelet method; Convergence acceleration; Sparse point representation

1. Introduction

Among the various phenomena modeled by partial differential or integral equations are countless instances where the mathematical solutions exhibit singularities [1, 2]. Those singularities are, in general, obstacles to the convergence of numerical approximation methods, in the sense that they may deteriorate the rate of the error decay with respect to the size of discrete problem. Achieving a precise accuracy where singularities exist would typically require finer resolution, and consequently, a heavier computational cost in comparison with the cases of smooth solutions. These problems result in the legitimate requirement of a special numerical method.

To offer accurate solutions with reasonable computational cost, an adaptive wavelet method appears as a natural solution. The crucial feature of the adaptive wavelet method is that it has the ability of representing the piecewise continuous functions accurately and efficiently. Then, it is possible to construct an adaptive dataset efficiently about a given solution by wavelet transformation. Considering that the majority of CFD solutions is piecewise continuous except for some discontinui-

ties such as shock, boundary layer, and vortex etc., this adaptability of wavelet method can present a useful advantage in terms of the efficiency.

In adaptive wavelet researches, there have been many successful attempts to apply wavelet method to CFD solution strategies. Holmström represents the algorithm for organizing sparse point representation (SPR) with an interpolating wavelet transformation [3]. Sjögreen uses a multi-resolution scheme to solve compressible Euler equations and also utilizes an interpolating wavelet transformation to construct the adapted dataset [4]. Kang et al. suggest a wavelet solution algorithm that solves the Euler equations much faster than a classical FVM solver based on the SPR method [5, 6].

Our target is the improvement of the computational efficiency for the Navier-Stokes equations while maintaining the accuracy of numerical schemes. For this, an adaptive wavelet method adequate for Navier-Stokes computation is developed by extending the Euler wavelet method of Kang et al. [5]. The method is based on the SPR method and includes the modified thresholding that maintains the spatial accuracy of a conventional solver by appropriate switching between threshold value and spatial truncation error. It also contains a stabilization technique which eliminates the additional numerical error due to thresholding. Numerical examples for the Navier-Stokes solution around a missile configuration are presented to verify

[†]This paper was recommended for publication in revised form by Associate Editor
Haecheon Choi

*Corresponding author. Tel.: +82 31 400 5289, Fax.: +82 31 406 5550
E-mail address: dohyung@hanyang.ac.kr

© KSME & Springer 2010

the efficiency enhancement of the method.

2. Sparse point representation

Wavelet transform has been found to be a practical tool in applied signal processing [7]. It was originally developed for feature extraction in image processing and for data compression. However, the modulated version of the wavelet method has been used to meet specific needs in the CFD field such as convergence acceleration of solution algorithm.

In this research, we use the adaptive wavelet method based on the SPR method with interpolating wavelet transformation [3]. A brief summary of the SPR method is as follows. First, assume a dyadic grid set presented as Eq. (1).

$$V_l = \{x_{l,k} \in R : x_{l,k} = 2^{-l}k, k \in Z\}, \quad l \in Z. \quad (1)$$

In the decomposition step, the dyadic dataset is decomposed into two types of coefficient as Eq. (2).

$$\begin{cases} \bar{f}_{l+1,2k} = f_{l,k} \\ \bar{f}_{l+1,2k+1} = P_{l+1,2k+1}(f_{l,k-\frac{p}{2}}, \dots, f_{l,k}, f_{l,k+1}, \dots, f_{l,k+\frac{p}{2}}) \end{cases} \quad (2)$$

where $P_{l,k}$ is the order of interpolating polynomial which is an even number. In the present research, we use 4th order of interpolating polynomial as Eq. (3).

$$\tilde{f}_{l+1,2k+1} = -\frac{1}{16}f_{l,k-1} + \frac{9}{16}f_{l,k} + \frac{9}{16}f_{l,k+1} - \frac{1}{16}f_{l,k+2}. \quad (3)$$

Then, the wavelet coefficients are defined as Eq. (4).

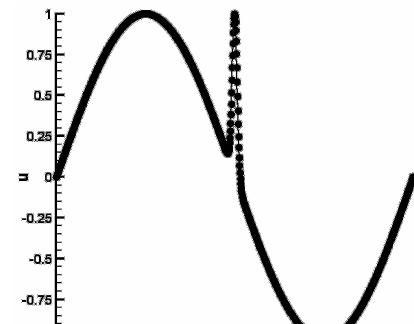
$$d_{l,k} = f_{l+1,2k+1} - \tilde{f}_{l+1,2k+1}, \quad \forall k \in Z. \quad (4)$$

In the thresholding process, the wavelet coefficients corresponding to regions of less importance are partially rejected; accordingly, a sparse wavelet representation is obtained.

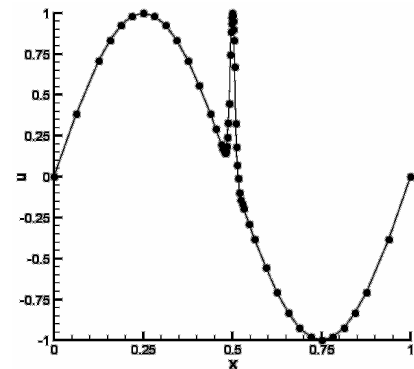
From the sparse wavelet representation, a compressed dataset is constructed with remaining points that correspond to significant wavelet coefficients. This compressed dataset is named as sparse point representation (SPR). The SPR is the set of function values that survive after thresholding, i.e., all the function values on the coarsest scale and the function values whose corresponding wavelet coefficient magnitude is greater than threshold value, ε . Here, the dataset contains the interpolation errors at the excluded points in the SPR and the maximum error is bounded within the order of ε as Eq. (5).

$$|d_{l,k}|_\infty = |f_{l,k} - \tilde{f}_{l,k}|_\infty < O(\varepsilon). \quad (5)$$

The SPR plays the role of adaptation to local solution characteristics by sorting out the points where classic solver is



(a) Original dataset (1,025 points)



(b) SPR dataset (57 points)

Fig. 1. Example of SPR method.

implemented. In general, smoothly changing a region results in quite small wavelet coefficients that are neglected in construction of the SPR. Thus, only a few points survive as the SPR dataset in the smooth region. On the other hand, the rapidly varying region produces much bigger wavelet coefficients and then most of the points remain in SPR dataset.

To test the SPR method, the test function is set as a superposition of a sine and a Gaussian as Eq. (6).

$$f(x) = \sin(2\pi x) + e^{-a(x-0.5)^2} \quad \text{with } a = 10,000. \quad (6)$$

It is smooth in most of the domain with a small interval of sharp variation and has 1,025 grid points with unit interval as shown in Fig. 1(a). After the SPR method, the remaining number of grid points is only 57 and the dataset follows the local features of solution as shown in Fig. 1(b). Also, the remaining number of grid points is small in the smooth region but large in the rapidly changing region.

3. Adaptive wavelet method

In the present research, the objective is the improvement of the computational efficiency of Navier-Stokes equations, while maintaining the numerical accuracy of conventional solvers. For that purpose, a modified threshold value is applied in order to maintain the spatial accuracy of conventional

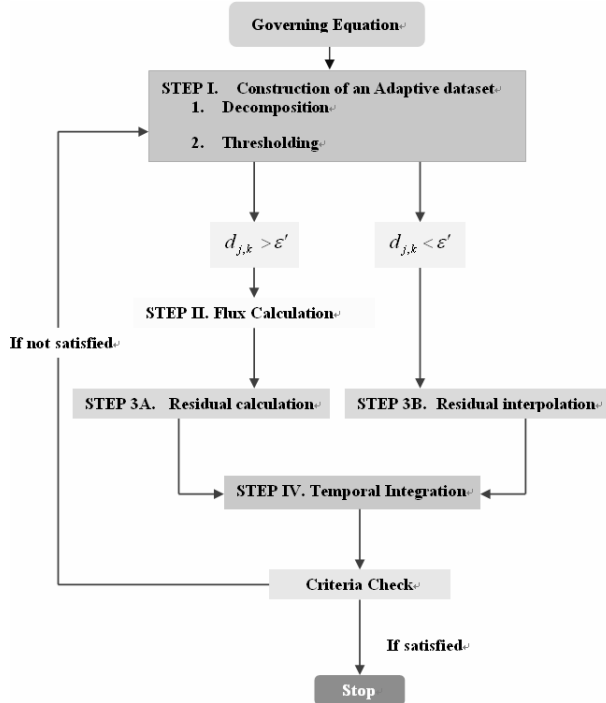


Fig. 2. Flow chart of the adaptive wavelet method.

CFD solvers. And a stabilization method is performed to stably construct an adaptive dataset while the compressibility of the adaptive wavelet method is enhanced. Also, residual interpolation is adopted at the n time step and time integration is performed on the entire domain. The flowchart in Fig. 2 shows the overall implementation of the new adaptive wavelet method in a reference Navier-Stokes solver. This implementation is comprised of the following sequential steps.

First, the two dimensional Navier-Stokes equations are given as Eq. (7).

$$\frac{\partial Q}{\partial t} + \frac{\partial E}{\partial x} + \frac{\partial F}{\partial y} = \frac{\partial E_v}{\partial x} + \frac{\partial F_v}{\partial y}$$

$$\text{with } Q = \begin{bmatrix} \rho \\ \rho u \\ \rho v \\ \rho e_t \end{bmatrix}, \quad E = \begin{bmatrix} \rho u \\ \rho u^2 + p \\ \rho u v \\ (\rho e_t + p)u \end{bmatrix}, \quad F = \begin{bmatrix} \rho v \\ \rho u v \\ \rho v^2 + p \\ (\rho e_t + p)v \end{bmatrix},$$

$$E_v = \frac{1}{\text{Re}} \begin{bmatrix} 0 \\ \tau_{xx} \\ \tau_{xy} \\ e_v \end{bmatrix}, \quad F_v = \frac{1}{\text{Re}} \begin{bmatrix} 0 \\ \tau_{xy} \\ \tau_{yy} \\ f_v \end{bmatrix}, \quad (7)$$

$$e_t = \frac{a^2}{\gamma(\gamma-1)} + \frac{1}{2}(u^2 + v^2), \quad e_v = u\tau_{xx} + v\tau_{xy} - q_x,$$

$$f_v = u\tau_{xy} + v\tau_{yy} - q_y$$

$$q_x = -\frac{\mu}{\text{Pr}(\gamma-1)} \frac{\partial T}{\partial x} \quad \text{and} \quad q_y = -\frac{\mu}{\text{Pr}(\gamma-1)} \frac{\partial T}{\partial y},$$

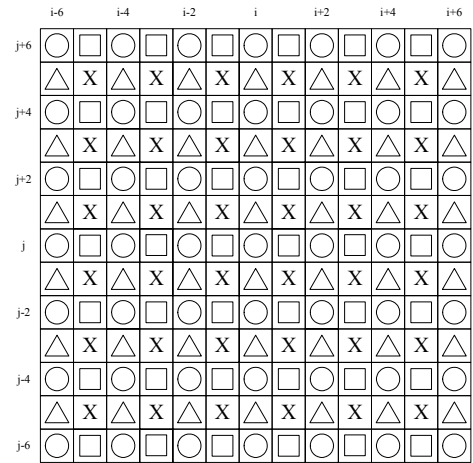


Fig. 3. Two dimensional dyadic gridset.

where all properties and governing equations are non-dimensionalized.

By coordinate transformation, Eq. (7) is rewritten as Eq. (8).

$$\frac{\partial \bar{Q}}{\partial \tau} = -\left[\frac{\partial \bar{E}}{\partial \xi} + \frac{\partial \bar{F}}{\partial \eta} - \frac{\partial \bar{E}_v}{\partial \xi} - \frac{\partial \bar{F}_v}{\partial \eta}\right] = -(R_{i,j}^n + R_{v,i,j}^n), \quad (8)$$

$$\text{with } \bar{Q} = \frac{Q}{J}, \quad \bar{E} = \frac{1}{J}[\xi_t + \xi_x E, +\xi_y F],$$

$$\bar{F} = \frac{1}{J}[\eta_t + \eta_x E_v, +\eta_y F_v], \quad \bar{E}_v = \frac{1}{J}[\xi_t + \xi_x E_v, +\xi_y F_v],$$

$$\bar{F}_v = \frac{1}{J}[\eta_t + \eta_x E_v, +\eta_y F_v], \quad R_{i,j}^n = \frac{\partial \bar{E}}{\partial \xi} + \frac{\partial \bar{F}}{\partial \eta},$$

$$R_{v,i,j}^n = \frac{\partial \bar{E}_v}{\partial \xi} + \frac{\partial \bar{F}_v}{\partial \eta}.$$

The first step is the construction of an adaptive dataset from flow variables, \bar{Q}^n by interpolating wavelet decomposition. If we assume a two-dimensional dyadic dataset as Fig. 3, positions of the symbol O are even numbered cells and the others of symbols □, △, and X are odd numbered cells. By using the 4th order interpolating polynomial, the values at the odd numbered cells are approximated from those of the even numbered cells as in Eq. (9).

$$\square: \tilde{Q}_{i+1,j}^n = -\frac{1}{16}Q_{i-2,j}^n + \frac{9}{16}Q_{i,j}^n + \frac{9}{16}Q_{i+2,j}^n - \frac{1}{16}Q_{i+4,j}^n,$$

$$\triangle: \tilde{Q}_{i,j+1}^n = -\frac{1}{16}Q_{i,j-2}^n + \frac{9}{16}Q_{i,j}^n + \frac{9}{16}Q_{i,j+2}^n - \frac{1}{16}Q_{i,j+4}^n, \quad (9)$$

$$\tilde{Q}_{i+1,j+1}^n = 0.5 \times \left(-\frac{1}{16}Q_{i-2,j-2}^n + \frac{9}{16}Q_{i,j}^n + \frac{9}{16}Q_{i+2,j+2}^n \right)$$

$$\text{X:} \quad -\frac{1}{16}Q_{i+4,j+4}^n + 0.5 \times \left(-\frac{1}{16}Q_{i-2,j+4}^n + \frac{9}{16}Q_{i,j+2}^n \right) \\ + \frac{9}{16}Q_{i+2,j}^n - \frac{1}{16}Q_{i+4,j-2}^n$$

Note that some indices of Q_{ij} are positioned outside of the domain at boundaries. To avoid this, odd numbered cells near

boundaries are always included in SPR dataset. After decomposition, wavelet coefficients at odd numbered cells are evaluated as Eq. (10).

$$\begin{aligned} \square: d_{i+1,j}^n &= Q_{i+1,j}^n - \tilde{Q}_{i+1,j}^n, \\ \triangle: d_{i,j+1}^n &= Q_{i,j+1}^n - \tilde{Q}_{i,j+1}^n, \\ X: d_{i+1,j+1}^n &= Q_{i+1,j+1}^n - \tilde{Q}_{i+1,j+1}^n. \end{aligned} \quad (10)$$

In the thresholding process, the wavelet coefficients are cut off when they are smaller than the threshold value, ε and the adapted dataset is constructed. However, this lossy omission of coefficients brings that the $O(\varepsilon)$ error due to thresholding is added to the solution. It may damage the numerical accuracy of a spatial scheme if the order is larger than that of truncation error of the scheme. To overcome this situation, we used the modified threshold value in order to maintain the l^{th} order of the spatial accuracy of CFD schemes as Eq. (11) [5, 6].

$$\varepsilon' = \min[\varepsilon, \Delta x']. \quad (11)$$

Then, $O(\varepsilon')$ error, which is smaller than the l -th order of the truncation error, is added to the solution. Based on this modified threshold value, ε' , the flag values of the cells are controlled. If the wavelet coefficient is larger than ε' , the cell is included in an adaptive dataset; if not, the cell is excluded from the dataset. Throughout this process, the dataset is adapted to the flow features while the spatial accuracy of conventional schemes is maintained.

However, an unexpected change in the SPR dataset may take place during the time marching and correspondingly, yield sudden ε' order of errors. These additional errors are transferred to the surroundings throughout the time integration step and deteriorate the whole solution. For the efficient computations, the sensitivity to the transient solution change due to $O(\varepsilon')$ error introduction should be diminished. To meet this purpose, the stabilization algorithm was suggested by Kang et al. [5, 6]. The detailed procedure of the algorithm is as follows:

Algorithm 1. Stabilization method for constructing an adaptive dataset

$Itag_{ij}$: Included positions in an adaptive dataset at n time step

$Itag_{I_{ij}}$: Included positions in an adaptive dataset at $n-1$ time step

```
Ctemp:|d_{ij}|  
do j:=1 to jmax  
do i:=1 to imax  
If(Ctemp > ε') then  
if(Itag_{I_{ij}} ≠ 1) then  
if(Ctemp > βε') then Itag_{ij}=1  
else Itag_{ij}=0
```

```
endif  
else Itag_{ij}=1  
endif  
else  
if(Itag_{I_{ij}}=1) then  
if(Ctemp < αε') then Itag_{ij}=0  
else Itag_{ij}=1  
endif  
else Itag_{ij}=0  
endif  
endif  
enddo  
enddo
```

Here, (α, β) is determined as (0.1, 10) for LU-SGS method and (0.2, 5) for 4th-order Runge-Kutta method [5, 6].

After construction of an SPR dataset, flux is evaluated depending upon the SPR dataset. Only when cells are included in the SPR dataset are the fluxes by using conventional spatial discretization schemes. In this research, AUSMPW+ is implemented, which is a highly accurate cell-centered finite volume scheme [8]. For the excluded points in the SPR dataset, rather inexpensive interpolation is adopted in evaluating residual values. If the flow feature changes largely at $n+1$ time step, the cells included in the adaptive dataset should change so as to follow the change of local flow features. However, due to thresholding at the n time step, the adapted dataset only includes information of the n time step. The solution's accuracy can be damaged because the flow variables are interpolated at the $n+1$ time step based on the adapted dataset at n time step. To get rid of these problems of the general wavelet method, residual interpolation is done at the n time step, instead of $n+1$ time step. The 4th order of interpolating polynomial in residual interpolation is presented in Eq. (12).

$$\begin{aligned} \square: \tilde{R}_{i+1,j}^n &= -\frac{1}{16} R_{i-2,j}^n + \frac{9}{16} R_{i,j}^n + \frac{9}{16} R_{i+2,j}^n - \frac{1}{16} R_{i+4,j}^n, \\ \triangle: \tilde{R}_{i,j+1}^n &= -\frac{1}{16} R_{i,j-2}^n + \frac{9}{16} R_{i,j}^n + \frac{9}{16} R_{i,j+2}^n - \frac{1}{16} R_{i,j+4}^n, \\ X: \tilde{R}_{i+1,j+1}^n &= 0.5 \times \left(-\frac{1}{16} R_{i-2,j-2}^n + \frac{9}{16} R_{i,j}^n + \frac{9}{16} R_{i+2,j+2}^n \right. \\ &\quad \left. - \frac{1}{16} R_{i+4,j+4}^n \right) + 0.5 \times \left(-\frac{1}{16} R_{i-2,j+4}^n + \frac{9}{16} R_{i,j+2}^n \right. \\ &\quad \left. + \frac{9}{16} R_{i+2,j}^n - \frac{1}{16} R_{i+4,j-2}^n \right) \end{aligned} \quad (12)$$

Finally time integration is carried out by either implicit or explicit method.

4. Numerical results and discussion

As an illustration of the accuracy and efficiency enhancement of the adaptive wavelet method, the flow around a missile is computed as the first case. For the conventional missile

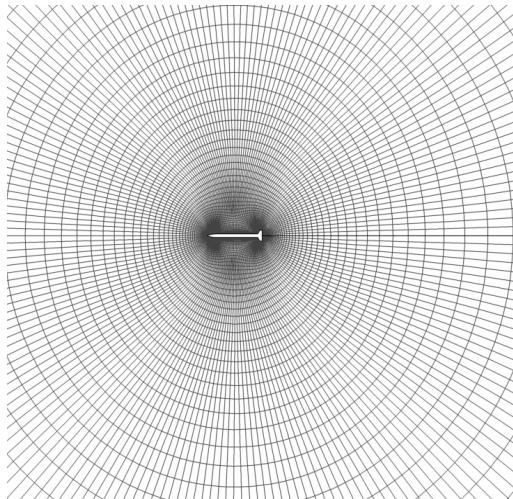


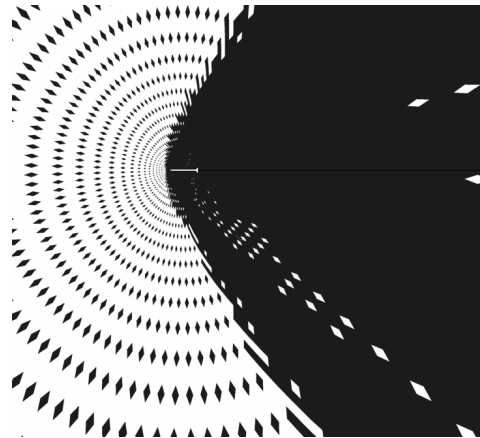
Fig. 4. Computational grid around a missile.

geometry with an O-give nose, a cylindrical body and fins is taken [9]. All the present computations on the missile are performed at a fixed free stream $M_\infty = 1.5$, angle of attack of $\alpha=5^\circ$ and Reynolds number of 100,000. The computational grid around a conventional missile is given in Fig. 4. For the assessment of stabilization of an adaptive dataset, 2nd-level resolution with threshold value of $\varepsilon=10^{-5}$ is applied. AUSMPW+ method [8] with 2nd-order MUSCL scheme is used for spatial discretization, while LU-SGS implicit method [10] and 4th-order Runge-Kutta method [11] are used for time integration.

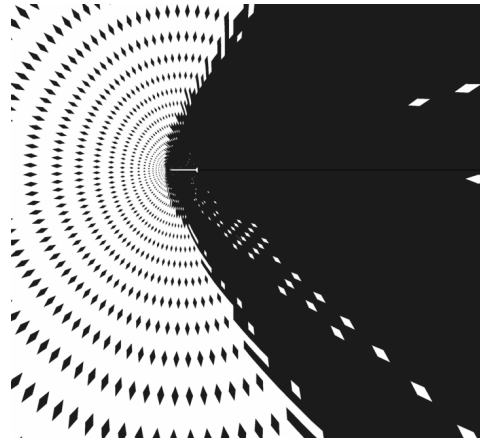
Compression ratios and effect of stabilization is shown in Figs. 5 and 6, respectively. From Fig. 5(a) and (b), we can observe the remaining grids in the adaptive dataset are much smaller when the stabilization algorithm is used. The extraction of cells from the adaptive dataset is strongly influenced by ε' order errors due to change of an adaptive dataset if the stabilization technique is not used. By the stabilization algorithm, the adaptive dataset is well constructed along with the local flow features. And the compression ratio is improved by about 40% with the stabilization algorithm as shown in Fig. 6.

Fig. 7 shows the pressure contours of a conventional solver and adaptive wavelet method using LU-SGS and Runge-Kutta time integration method, respectively. Fig. 8 shows Mach number contours of the conventional solver and of the adaptive wavelet method using LU-SGS and Runge-Kutta time integration methods, respectively. It can be known that the contours of conventional solvers and adaptive wavelet method are almost the same.

Table 1 presents the overall efficiency enhancement of the adaptive wavelet method. In Table 1 the difference of lift coefficients associated with each solution has a similar order and changes within 2nd-order of accuracy. Adaptive method with 2nd-level resolution is taking less CPU time for Runge-Kutta and 3rd-level resolution is taking less time for LU-SGS. It can be concluded that if the number of the grid points is not sufficient to define the flow physics accurately, we will get no



(a) Stabilization off



(b) Stabilization on

Fig. 5. Adative dataset w/ and w/o stabilization.

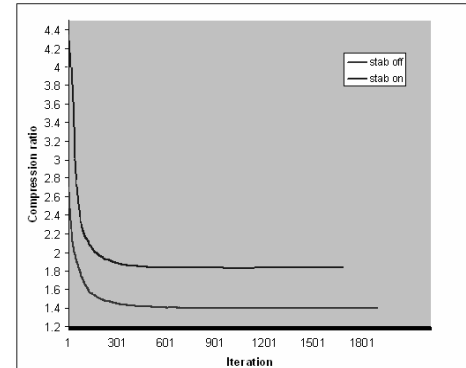
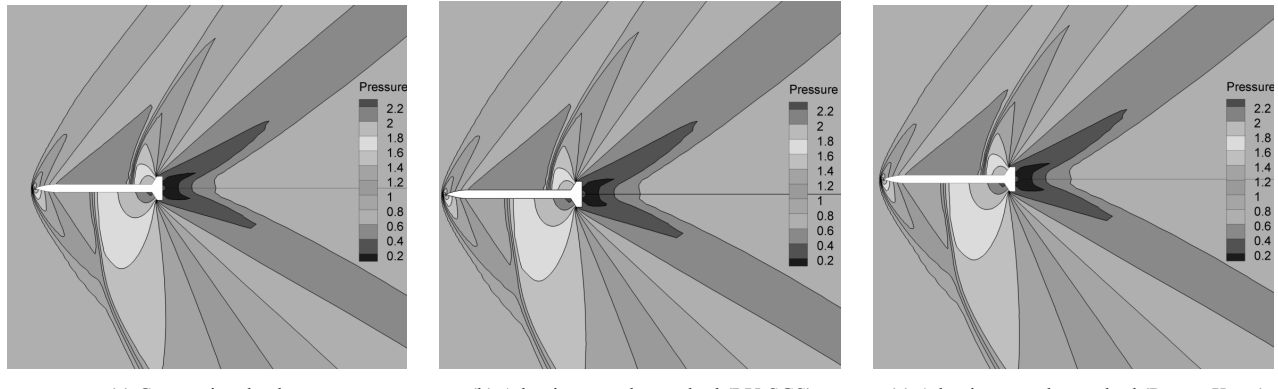
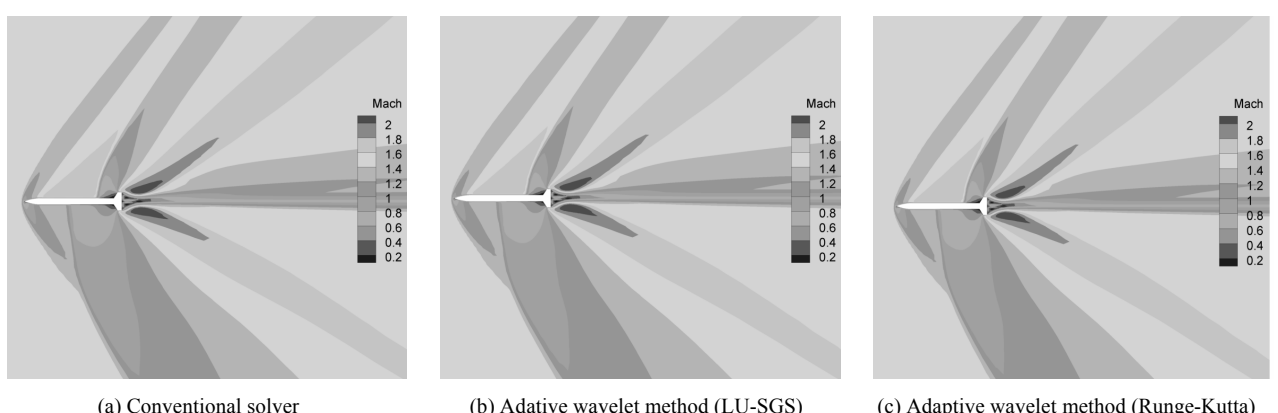


Fig. 6. Effect of the stabilization on the compression ratio of the adaptive wavelet method.

improvement in convergence acceleration by simply increasing the resolution level. Runge-Kutta is shown to provide faster convergence than LU-SGS. The reason is that most of the computing time is dedicated to evaluating fluxes, and the Runge-Kutta method is fast in this respect. Using LU-SGS improves the computational efficiency by 61%, while for Runge-Kutta method it is given as 110%.

Table 1. Results for conventional missile.

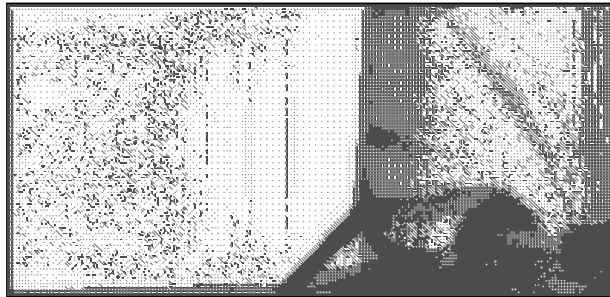
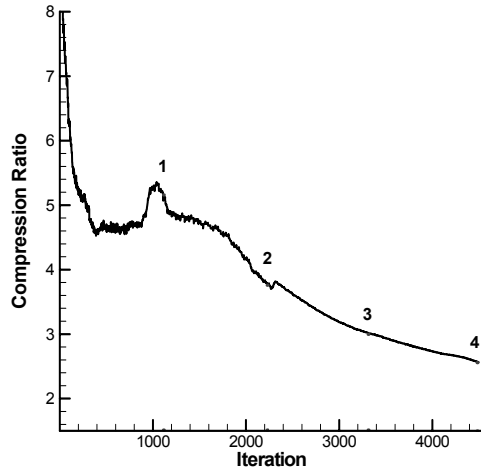
Missile	Time Integration	Wavelet Decomposition Level	Iteration	CPU Time	Time Ratio	Lift Coefficient	Difference (%)
	LU-SGS	Conventional	4366	495	1	0.5352	
		Level 1	2866	317	1.562	0.5332	0.3801
		Level 2	2871	310	1.597	0.5332	0.3791
		Level 3	2873	306	1.618	0.5331	0.3890
	4 th Order Runge-Kutta	Conventional	3219	669	1	0.5353	
		Level 1	1894	348	1.922	0.5317	0.6608
		Level 2	1927	318	2.104	0.5320	0.6076
		Level 3	1915	322	2.077	0.5316	0.6930

Fig. 7. Pressure contours for a conventional missile computation ($M = 1.5$, $Re = 10^5$).Fig. 8. Mach number contours for conventional missile ($M = 1.5$, $Re = 10^5$).

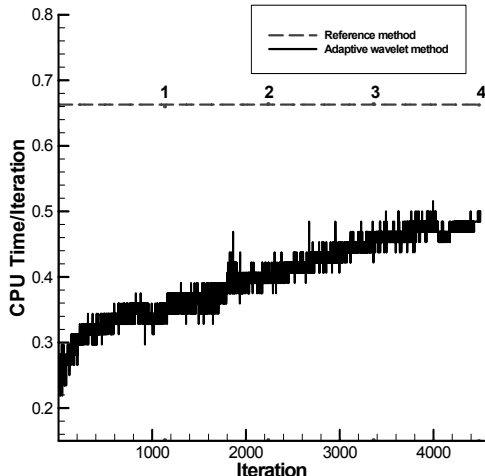
For the second test, the new adaptive wavelet method is applied to the two-dimensional viscous shock tube problem [12]. The computational domain is set to be $0 \leq x \leq 1$, $0 \leq y \leq 0.5$, and the total number of grids points is set at 401×201 . For boundary conditions, symmetric boundary conditions are applied at $y = 0.5$. And at the other sides, wall boundary conditions are enforced. The initial conditions of this problem are given as Eq. (13).

$$\begin{aligned}
 (\rho, u, v, p) &= (120, 0, 0, \frac{120}{\gamma}) \text{ where } 0 \leq x \leq 0.5, 0 \leq y \leq 0.5, \\
 (\rho, u, v, p) &= (1.2, 0, 0, \frac{1.2}{\gamma}) \text{ where } 0.5 < x \leq 1, 0 \leq y \leq 0.5, \\
 \text{with } \gamma &= 1.4, \text{ Re} = 200, \text{ and } \mu = \text{constant}.
 \end{aligned} \quad (13)$$

Here, inviscid fluxes are discretized by AUSMPW+ and MUSCL scheme with van Leer limiter [8]. Viscous fluxes are

Fig. 9. Adaptive dataset of viscous shock tube problem at $t=1$ sec.

(a) Variation of compression ratio



(b) Variation of CPU time/iteration

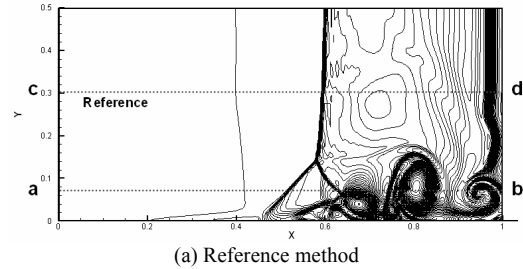
Fig. 10. Variation of compression ratio and CPU time/iteration of viscous shock tube problem.

calculated by the 2nd-order of spatial accuracy. For a time integration, the 4th-order of Runge-Kutta method [11] with the CFL number of 0.4 is implemented and ε is set as 10^{-5} . The stabilization method is also used for enhancing the compression ratio.

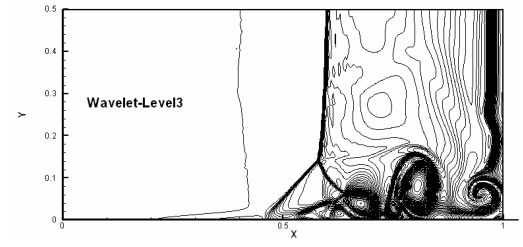
Fig. 9 shows the adaptive dataset of 3 levels of wavelet

Table 2. Results for viscous shock-tube problem.

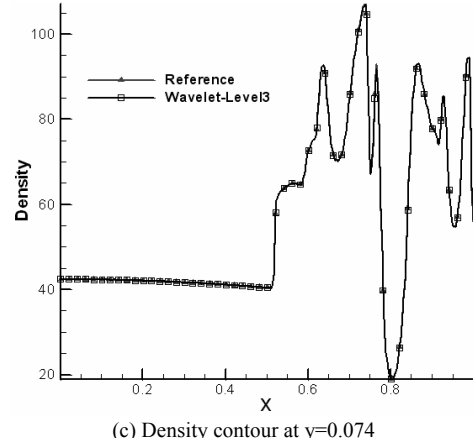
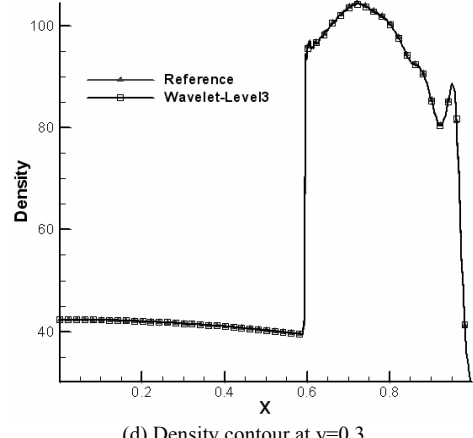
Wavelet Decomposition Level	Iteration	CPU Time	Time Ratio
Reference		2982.81	
Level 1	5.57E-06	2287.41	1.30
Level 2	5.34E-06	1805.17	1.65
Level 3	6.63E-06	1732.97	1.72



(a) Reference method



(b) Adaptive wavelet method

(c) Density contour at $y=0.074$ (d) Density contour at $y=0.3$ Fig. 11. Density contours of viscous shock tube problem at $t=1$ sec.

transformation at 1 second. At the beginning, a strong shock is propagated to the right wall, and then reflected and re-propagated again to the left accompanying complex shock-shear-boundary layer interactions. The adaptive dataset is seen to follow the flow feature effectively; near shock discontinuities and the vortex region, there remain many grid points to manifest the crucial features of the solution.

Fig. 10 shows the variation of compression ratio and CPU time/iteration according to time marching, respectively. Due to the moving shock and interactions between the shock and the boundary layer, the flow features become very complex as time goes further. Therefore, a large number of points remain in the adaptive dataset to represent properly these features. Accordingly, the compression ratio decreases, which results in the continuous increase of CPU time/iteration. Based on these results, the computation becomes 1.7 times faster than that of the reference solver in maximum. The L2 error between the solutions of the reference solver and the new adaptive wavelet method is evaluated as 6.63×10^{-6} . The overall efficiency improvement and L2 error according to the wavelet decomposition level is summarized in Table 2.

In Fig. 11, the density contours of the reference solver and the new adaptive wavelet method are presented at 1 second. The comparison of density contours at $y=0.074$ (a-b line) and $y=0.3$ (c-d line) is presented in Fig. 11(c) and (d), respectively. It is shown that density distributions are exactly matched with the new adaptive wavelet method.

5. Conclusions

The adaptive wavelet method is proposed for the efficiency enhancement of a Navier-Stokes solver. By applying the threshold value modification, stabilization procedure and residual interpolation in the computation of the Navier-Stokes problems, the numerical accuracy is preserved even with increase of the computational efficiency. With maintenance of solution accuracy, the computation becomes 1.62 times faster in the LU-SGS implicit method and 2.1 times faster in the Runge-Kutta explicit method than the conventional solvers in the missile problem. Also in the viscous shock tube problem, the computation is 1.7 times faster than the conventional solver. The proposed adaptive wavelet method is expected to show significant efficiency improvement as well as accuracy preservation in various practical applications that involves even various singularities such as vortices and jet.

Acknowledgment

This work supported by Research Program supported by the This work was supported by the Korea Research Foundation (KRK-2007-521-D00070) and the second stage of the Brain Korea 21 Project in 2009.

Nomenclature

a : Speed of sound

$d_{l,k}$: Wavelet coefficient at $x_{l,k}$
$d_{i,j}^n$: Wavelet coefficient at (i,j) cell of n time step
$f_{l,k} = f(x_{l,k})$: Exact functional value at $x_{l,k}$
$\tilde{f}_{l,k} = \tilde{f}(x_{l,k})$: Interpolated value given by the interpolating subdivision scheme
$L_{i,j}^n$: (ρ, p, u, v) at (i,j) cell of n time step
$\tilde{L}_{i,j}^n$: Interpolated value of $L_{i,j}^n$ given by interpolating subdivision scheme
p	: Pressure
$P_{l+1,2k+1}$: Interpolating polynomial
$R_{i,j}^n$: Residual values at (i,j) cell of n time step
$\tilde{R}_{i,j}^n$: Interpolated value of $R_{i,j}^n$ given by interpolating subdivision scheme
u, v	: Components of the velocity vector
V_i	: Dyadic grid set
$x_{l,k}$: k^{th} cell on V_i

Subscript

i, j	: Position of a cell
L	: Wavelet resolution level
K	: Position of the cell

Superscript

n	: Current time step
-----	---------------------

Greek

ε	: Threshold value
ε'	: Modified threshold value
γ	: Ratio of specific heat (1.4 for air)
ρ	: Density

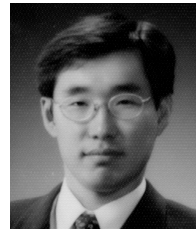
References

- [1] A. Harten, Adaptive multiresolution schemes for shock computation, *Journal of Computational Physics*, 115 (1994) 319-338.
- [2] H. Kang, D. Lee and D. Lee, A study on CFD Data Compression using Hybrid Supercompact Wavelets, *Journal of Mechanical Science and Technology (KSME International Journal)*, 17 (11) (2003) 1784-1792.
- [3] M. Holmström, Solving Hyperbolic PDEs Using Interpolating Wavelets, *SIAM Journal on Scientific*, 21 (1999) 405-420.
- [4] B. Sjögreen, Numerical Experiments with the Multiresolution Scheme for the Compressible Euler Equations, *Journal of Computational Physics*, 117 (1995) 251-261.
- [5] H. Kang, K. Kim, D. Lee and D. Lee, Improvement in computational efficiency of Euler equations via a modified Sparse Point Representation method, *Computers & Fluids*, 37 (2008) 265-280.
- [6] H. Kang, D. Lee, K. Kim and D. Lee, Improved Computational Efficiency of Unsteady Flow Problems via the Modified Wavelet Method, *AIAA Journal*, 46 (2008) 1191-1203.

- [7] Y. Nievergelt, Wavelet made easy, Birkhäuser, Boston · Basel · Berlin, 1999.
- [8] K. Kim, C. Kim and O. Rho, Methods for the Accurate Computations of Hypersonic Flows: I. AUSMPW+Scheme, *Journal of Computational Physics*, 174 (2001) 38-80.
- [9] E. Oktay, N. Alemdaroglu, E. Tarhan and P. Champigny, Unstructured Euler solutions for missile aerodynamics, *Aerospace Science and Technology*, 4 (2000) 453-461.
- [10] S. Yoon and A. Jameson, Lower-upper Symmetric-Gauss-Seidel method for the Euler and Navier-Stokes equations, *AIAA Journal*, 26 (1988) 1025-1026.
- [11] A. Jameson, W. Schmidt and E. Turkel, Numerical solution of the Euler equations by finite volume methods using Runge-Kutta time-stepping schemes, *AIAA 14th fluid and plasma dynamics conference*, (1981) 23-25.
- [12] B. Sjögreen and H. C. Yee, Grid convergence of high order methods for multiscale complex unsteady viscous compressible flows, *Journal of Computational Physics*, 185 (2003) 1-26.



Hyungmin Kang is currently a Post Doc. at Seoul National University. His B.S., M.S. and Ph.D. are from Seoul National University.



Dohyung Lee is a professor at Mechanical Engineering Department of Hanyang University. He is also consulting professor at NASA Ames Research Center and associate editor of the Journal of Mechanical Science and Technology.